

L.E. Zakharov et al.

Electromagnetic Thin Wall Model for Simulations of Plasma Wall Touching Kink and Vertical Modes

Preprint of Paper to be submitted for publication in
Journal of Plasma Physics

“This document is intended for publication in the open literature. It is made available on the clear understanding that it may not be further circulated and extracts or references may not be published prior to publication of the original when applicable, or without the consent of the Publications Officer, EUROfusion Programme Management Unit, Culham Science Centre, Abingdon, Oxon, OX14 3DB, UK or e-mail Publications.Officer@euro-fusion.org”.

“Enquiries about Copyright and reproduction should be addressed to the Publications Officer, EUROfusion Programme Management Unit, Culham Science Centre, Abingdon, Oxon, OX14 3DB, UK or e-mail Publications.Officer@euro-fusion.org”.

The contents of this preprint and all other EUROfusion Preprints, Reports and Conference Papers are available to view online free at <http://www.euro-fusionscipub.org>. This site has full search facilities and e-mail alert options. In the JET specific papers the diagrams contained within the PDFs on this site are hyperlinked.

Electromagnetic Thin Wall Model for Simulations of Plasma Wall Touching Kink and Vertical Modes

Leonid E. Zakharov^{1†}, Calin V. Atanasiu², Karl Lackner³, Matthias Hoelzl³ and Erika Strumberger³

¹LiWFusion, PO Box 2391, Princeton, New Jersey, 08543

²National Institute for Laser, Plasma and Radiation Physics, Atomistilor 409, PO Box MG-36, 077125 Magurele, Bucharest, Romania

³Max Planck Institute for Plasma Physics, Boltzmannstr. 2, 85748 Garching, Germany

(Received xx; revised xx; accepted xx)

The understanding of plasma disruptions in tokamaks and predictions of their effects require realistic simulations of electric currents excitation in 3-dimensional vessel structures by the plasma touching the walls. As it was discovered at JET in 1996 (Litunovski 1995; Noll *et al.* 1996) the wall touching kink modes are frequently excited during the Vertical Displacement Events (VDE) and cause big sideways forces on the vacuum vessel which are difficult to confront in large tokamaks. In disruptions, the sharing of electric current between the plasma and the wall plays an important role in plasma dynamics and determines the amplitude and localization of the sideways force (Riccardo, Noll *et al.* 2000; Riccardo and Walker 2000; Zakharov 2008; Riccardo *et al.* 2009; Bachmann *et al.* 2011). This paper describes a flat triangle representation of electric circuits of a thin conducting wall of arbitrary 3-dimensional geometry. Implemented into the Shell Simulation Code (SHL) and the Source Sink Current code (SSC), this model is suitable for modelling the electric currents excited in the wall inductively and through the current sharing with the plasma.

1. Introduction

Recent progress in theoretical understanding of so-called Asymmetric Vertical Displacement Events (AVDE) in tokamaks is related with the theory of Wall Touching Kink Modes and Wall Touching Vertical Magneto-Hydrodynamic Modes (WTKM, WTVM) (Zakharov 2008; Zakharov *et al.* 2012; Gerasimov *et al.* 2014; Xiong *et al.* 2015; Gerasimov *et al.* 2015). At JET tokamak, during upward plasma motion due to vertical instability, a kink mode $m/n = 1/1$ (m, n are poloidal and toroidal wave numbers) is typically excited and plasma touches the wall shares the electric current with it. This current stabilizes the fast development of the kink mode but at the same time generates big sideways forces on the vacuum vessel, which are difficult to confront (Litunovski 1995; Noll *et al.* 1996). The projection of these forces at ITER in 2007 caused modifications in the design support structures of its vacuum vessel.

The theory of WTKM (Zakharov 2008; Zakharov *et al.* 2012) explained an unexpected sign of the currents in the wall during AVDE, which are opposite in direction to the plasma current in all JET upward Vertical Displacement Events (VDE). The engineering scaling (Noll *et al.* 1996) of sideways forces was confirmed. Recently, the

† Email address for correspondence: lzakharov@comcast.net

same theory provides an interpretation of the toroidal asymmetry of diamagnetic signal during excitation of the WTKM. Theory also predicted the excitation of currents opposite to plasma current in pure axisymmetric VDEs and motivated the installation of a special tile diagnostics on the EAST tokamak. The EAST measurement confirmed the theory prediction (Xiong *et al.* 2015).

The theoretical understanding of VDE disruption was formalized by creation of the Tokamak Magneto-Hydro-Dynamic (TMHD) model, which considers the disruption as fast equilibrium evolution. The MHD plasma instability in tokamaks always generates surface currents at the plasma edge. In VDE disruptions the fast instability growth is prevented by the plasma contact with the wall when the surface currents from the leading edge of the plasma are transferred to the wall. These currents, called Hiro currents, are opposite always in direction to the plasma current. They balance the instability and convert it into fast equilibrium evolution. In the case of pure axisymmetric VDE disruptions the Hiro currents flow in toroidal direction along the plasma facing wall surface. If necessary, they shortcut the gaps between the plasma facing in-vessel tiles. In AVDE with a $m/n = 1/1$ plasma deformation, the Hiro currents are shared between the plasma edge and the wall. A specific dynamic Scrape off Layer disruption (DSoL) is created in order to conduct the Hiro currents from the plasma surface to the wetting zone of the plasma contact with the wall.

Another type of currents are created due to shrinkage of the plasma cross-section and releasing charged particles from the core to the open field lines. Accordingly, these particles create a conventional (although 3-dimensional) Scrape off layer SoL around the plasma core and DSoL. The loop voltage drives these SoL currents, called Evans currents (introduced by theory instead of controversial “halo” currents) to the wall. The Evans currents are source limited by particle supply from the core and play a minor role in disruptions.

The TMHD theory associates the triggering of thermal quench by 3-D perturbation of magnetic configuration caused by the plasma contact with the wall. Also the excitation of Hiro currents in the wall is considered as a reason of typical negative loop voltage spike measured at the beginning of the disruptions.

All new physics effects related to a direct contact of the plasma with the wall and to the current sharing require their implementation into plasma-wall simulations. This paper provides an initial step in implementation of the 3-D wall into TMHD model (Zakharov *et al.* 2015). The Units used in the paper are: m, T, MA, MN, MPa, $10^6 \Omega^{-1} \text{m}^{-1}$, $\mu_0 = 0.4\pi$ for lengths, magnetic fields, currents, forces, pressure, electric conductivity and magnetic permeability correspondingly.

The thin wall approximation is the simplest model for describing the effect of a conducting shell on the plasma dynamics. This model replaces the real current distribution in the bulk of the structure by a sheet current along the plasma facing surface. First it is reasonable for thin stainless steel (SS) structures of the vacuum vessel (of about 1-3 cm thick) which have the electric conductivity 1.38. The current penetration time through the thickness h of the wall $\tau_{h^2} \equiv \mu_0 \sigma h^2 / 4$ for SS can be assessed $\tau_{h^2}^{SS} \simeq 0.4 \cdot 10^{-4} h_{cm}^2$. This means that for disruption processes, which are typically longer than 1 ms, the currents excited in the SS shell will be uniformly distributed across the shell thickness.

The thin wall model might be questionable in the presence of the copper passive structures inside the vacuum vessel as in the EAST tokamak (Xiong *et al.* 2015). For copper, whose electric conductivity is 58.8, the current penetration time $\tau_{h^2}^{Cu} \simeq 1.8 \cdot 10^{-3} h_{cm}^2$ and is comparable with the duration of the VDE on EAST $\simeq 10$ ms ($h = 2$ cm). Still, the thickness of the copper shell is small relative to the plasma size and the thin wall model could be a good reference model for simulations.

Another example of effects, which are not reproduced by the thin wall approximation, is the penetration of the magnetic field through the gaps between highly conducting plates whose thickness is comparable or bigger than the width of the gap. Having this in mind, the corrections to the thin wall model should be made for such cases.

The advantage of the triangle representation of the curved geometry of the plasma facing wall surface resides in its simplicity and universal applicability. Another significant advantage of this geometrical model is the existence of analytical formulas for the magnetic field of a uniform current in a single triangle. The 3-dimensional thin wall model complements the Tokamak Magneto-Hydro-Dynamics (TMHD) disruption model (Zakharov *et al.* 2015) by the wall response.

The paper describes the implementation of the thin wall model into two mutually linked codes: (a) SHL (shell simulation code) for simulations of eddy currents, and (b) SSC (source/sink code) for simulating current sharing between the plasma and the wall. §2 presents the differential equations for the surface currents determination in a thin wall. §3 describes the current representation inside a single triangle. §4 gives the energy principles for defining of a finite element representation of equations, while §5 presents the matrix form of these principles. §6 shows the examples of simulation of thin wall currents by SSC and SHL codes. The comparison of newly developed SSC-code with analytical solutions is given in §7. A step toward modeling the Wall Touching Kink Modes is given in §8. §9 presents a potential optimization of thin wall problem by localization of the region for the source/sink currents. The Summary is given in §10.

2. Two kinds of surface currents in the thin wall

For the purpose of TMHD modeling, the surface current density $h\mathbf{j}$ in the conducting shell (h is the thickness of the current distribution) can be split into two components: (a) one is a divergence free surface current \mathbf{i} and (b) the second one is a current $\propto -\nabla\phi^S$ with potentially finite divergence in order to describe the current sharing between the plasma and the wall:

$$h\mathbf{j} = \mathbf{i} - \bar{\sigma}\nabla\phi^S, \quad \mathbf{i} \equiv \nabla I \times \mathbf{n}, \quad (\nabla \cdot \mathbf{i}) = 0, \quad \bar{\sigma} \equiv h\sigma. \quad (2.1)$$

Here, I is the stream function of the divergence free component and \mathbf{n} the unit normal vector to the wall. The \mathbf{i} component corresponds to well-known eddy currents. Following V.Riccardo (Riccardo, Noll *et al.* 2000), we refer the second component $-\bar{\sigma}\nabla\phi^S$ as the source/sink current, or S/S-current. Accordingly, the surface function ϕ^S is called the source/sink potential.

The S/S-current in Eq. (2.1) is the surface current originated from the sharing of the electric current between the plasma and the wall. It is determined from the following equation

$$(\nabla \cdot (h\mathbf{j})) = -(\nabla \cdot (\bar{\sigma}\nabla\phi^S)) = j_{\perp}, \quad j_{\perp} \equiv -(\mathbf{j} \cdot \mathbf{n}) = j_{\perp}^{Hr} + j_{\perp}^{Ev}, \quad (2.2)$$

where j_{\perp} is the density of the current coming from/to the plasma and acting as a galvanic source for the surface currents on the wall. The sign of j_{\perp} is positive for the current from the plasma to the wall, which corresponds to the source. The part j_{\perp}^{Hr} of j_{\perp} can be associated with the Hiro currents, which are excited inductively due to plasma deformation and its contact with the wall. The amplitude of the Hiro currents is not sensitive to the details of plasma-wall interaction (the instability acts as a current generator). For wall simulations these currents and their wetting zone can be considered to be given. The TMHD disruption model splits the equation of motion into an equilibrium equation and the plasma advancing equation. The splitting allows disruption

simulations on a relatively slow time scale in comparison with the fast time of ideal MHD instabilities (Zakharov *et al.* 2015). In a thin DSoL approximation (the δ -functional Hiro currents) the equilibrium equation determines the shape of the contact zone, the contour of the entrance and the amplitude of the Hiro currents along this contour. The more realistic model should include the finite thickness of DSoL and an additional edge physics which determines the structure of DSoL.

Another, j_{\perp}^{Ev} , part of j_{\perp} is associated with the Evans currents in the conventional SoL (Zakharov *et al.* 2012; Zakharov *et al.* 2015)) created by the plasma particles released from the shrinking plasma core when the plasma touches the material surface. The toroidal loop voltage drives the current in this SoL along the open field lines. This current is “source” limited by the rate of the electric charge release edN/dt , where N is the number of particles in the plasma core. Unlike the Hiro currents, which are an inductive effect of instability, the Evans currents represent a side “resistive” effect which depends on plasma-wall interactions. Being force-free, these currents do not affect the disruption dynamics. But they can be measured and should be simulated, thus providing the information on plasma-wall interaction during disruptions.

Both Hiro and Evans currents from the SoL enter the wall surface in the vicinity of the contour of the wetting zone, whose geometry is determined by the plasma dynamics. The value of the Hiro currents is determined dynamically by the plasma deformation and flux conservation. The waveform of the total Evans current $I^{Ev}(t)$ is considered as input. In a thin DSoL and SoL approximation, which would be a simplest reasonable model, the current density j_{\perp} can be considered as δ -functional along the wetting zone contour. In this paper for demonstration of the capabilities of the numerical codes, a distributed over wetting zone j_{\perp} -profiles are used.

In terms of components of the surface current Faraday’s law can be written as

$$-\frac{\partial \mathbf{A}}{\partial t} - \nabla \phi^E = \bar{\eta}(\nabla I \times \mathbf{n}) - \nabla \phi^S, \quad \bar{\eta} \equiv \frac{1}{\bar{\sigma}}. \quad (2.3)$$

Here, \mathbf{A} is the vector potential of the magnetic field and ϕ^E is the electric potential. The effective resistance $\bar{\eta}$ is introduced for convenience.

The normal component of the curl of this equation gives the equation for the stream function I (Tseitlin 1970; Chance 1997; Chance *et al.*, 2002; Chu *et al.*, 2003; In 2006; Pustovitov 2008; Strumberger *et al.* 2008; Atanasiu *et al.* 2009, 2013)

$$(\nabla \cdot (\bar{\eta} \nabla I)) = \frac{\partial B_{\perp}}{\partial t} = \frac{\partial (B_{\perp}^{pl} + B_{\perp}^{coil} + B_{\perp}^I + B_{\perp}^S)}{\partial t}. \quad (2.4)$$

In the right hand side the normal component of the magnetic field is represented by separate contributions from the plasma B_{\perp}^{pl} , external coils B_{\perp}^{coil} , and from two components of the surface current, B_{\perp}^I and B_{\perp}^S , respectively.

Two equations (2.2,2.4) describe the current distribution in the thin wall given the sources j_{\perp} , B_{\perp}^{pl} , B_{\perp}^{coil} specified as functions of space and time. In addition to Eqs. (2.2,2.4) the expression for the magnetic field from the surface current (e.g., Bio-Savart formulas) has to be specified in order to close the system of equations. The important property of this system of equations is the independence of equation (2.2) for ϕ^S from equation (2.4). Solved independently, it contributes via the term $\partial B^S / \partial t$ to the right hand side of Eq. (2.4).

Equations (2.2,2.4) can be solved using the finite difference method, e.g., as in Ref. (Atanasiu *et al.* 2013) for simulation of the thin wall response to the perturbations from a rotating kink mode. In this paper the implementation of a more universal method is described.

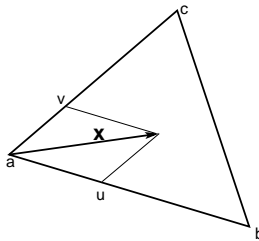


FIGURE 1. Elementary triangle

3. Triangle model for two kinds of surface currents in the wall

The triangle electromagnetic representation of the thin wall is based on the following expressions for the vector potential \mathbf{A} and magnetic field \mathbf{B} of a uniform surface current $\mathbf{i}=\text{const}$ inside the triangle

$$\mathbf{A}(\mathbf{r}) = h\mathbf{j}\varphi(\mathbf{r}) = [(\nabla I \times \mathbf{n}) - \bar{\sigma}\nabla\phi^S]\varphi(\mathbf{r}), \quad \varphi(\mathbf{r}) \equiv \int \frac{dS'}{X}, \quad (3.1)$$

$$\mathbf{B}(\mathbf{r}) = (h\mathbf{j} \times \mathbf{e}) = \{[(\nabla I \times \mathbf{n}) - \bar{\sigma}\nabla\phi^S] \times \mathbf{e}\}, \quad \mathbf{e}(\mathbf{r}) \equiv \int \frac{\mathbf{X}}{X^3} dS', \quad (3.2)$$

$$\mathbf{X} \equiv \mathbf{r} - \mathbf{r}', \quad X \equiv |\mathbf{r} - \mathbf{r}'|, \quad (3.3)$$

where φ is the electric potential of a triangle with a uniform unit charge, \mathbf{e} is its electric field, \mathbf{r}, \mathbf{r}' are the coordinates of the observation and the source points, and the integrals are taken over the surface of the triangle. Both φ and \mathbf{e} have analytical expressions in terms of elementary functions.

In 2008 the triangle based electro-dynamic model of the thin wall was implemented into the numerical Shell simulation code (SHL), mentioned in Ref. (Zakharov *et al.* 2012) and used for simulations of eddy currents in the Lithium Tokamak Experiment (LTX) (Berzak Hopkins *et al.* 2012). Earlier, the triangle based wall model was implemented in STARWALL code of P. Merkel (Merkel *et al.* 2004, 2006; Strumberger *et al.* 2008; Merkel *et al.* 2015) for resistive wall mode studies.

Inside a triangle with vertices a, b, c (Fig. 1) the edges and the local vector of an arbitrary point are defined as

$$\mathbf{x} \equiv \mathbf{r} - \mathbf{r}_a, \quad \mathbf{r}_{ba} \equiv \mathbf{r}_b - \mathbf{r}_a, \quad \mathbf{r}_{cb} \equiv \mathbf{r}_c - \mathbf{r}_b, \quad \mathbf{r}_{ac} \equiv \mathbf{r}_a - \mathbf{r}_c. \quad (3.4)$$

For calculations of the finite elements, new coordinates u, v with the origin in the vertex a are introduced by

$$\mathbf{x}(u, v) \equiv \mathbf{r}_{ba}u - \mathbf{r}_{ac}v, \quad \mathbf{x}(0, 0) = 0, \quad \mathbf{x}(1, 0) = \mathbf{r}_{ba}, \quad \mathbf{x}(0, 1) = -\mathbf{r}_{ac}. \quad (3.5)$$

The metric tensor is determined by the element of length dl

$$d\mathbf{x}(u, v) = \mathbf{r}_{ba}du - \mathbf{r}_{ac}dv, \quad dl^2 = g_{uu}du^2 + 2g_{uv}dudv + g_{vv}dv^2, \quad (3.6)$$

$$g_{uu} = |\mathbf{r}_{ba}|^2, \quad g_{uv} = -(\mathbf{r}_{ba} \cdot \mathbf{r}_{ac}), \quad g_{vv} = |\mathbf{r}_{ac}|^2. \quad (3.7)$$

Its Jacobian D is given by

$$D^2 = g_{uu}g_{vv} - g_{uv}^2 = |\mathbf{r}_{ba}|^2|\mathbf{r}_{ac}|^2 - (\mathbf{r}_{ba} \cdot \mathbf{r}_{ac})^2, \quad D = |(\mathbf{r}_{ba} \times \mathbf{r}_{ac})| \quad (3.8)$$

and is equal to the doubled surface area of the triangle $D = 2S$

$$2S = |(\mathbf{r}_{ba} \times \mathbf{r}_{ac})|, \quad \mathbf{n} \equiv \frac{(\mathbf{r}_{ac} \times \mathbf{r}_{ba})}{2S}. \quad (3.9)$$

The gradients of u, v are given by

$$\nabla u = \frac{(\mathbf{n} \times \mathbf{r}_{ac})}{(\mathbf{n} \cdot (\mathbf{r}_{ac} \times \mathbf{r}_{ba}))} = \frac{(\mathbf{n} \times \mathbf{r}_{ac})}{D}, \quad \nabla v = \frac{(\mathbf{n} \times \mathbf{r}_{ba})}{(\mathbf{n} \cdot (\mathbf{r}_{ac} \times \mathbf{r}_{ba}))} = \frac{(\mathbf{n} \times \mathbf{r}_{ba})}{D}. \quad (3.10)$$

The plane functions I, ϕ^S inside the triangle are defined by their values $I_a, I_b, I_c, \phi_a^S, \phi_b^S, \phi_c^S$ in vertexes as linear functions of u, v

$$I = I_a + (I_b - I_a)u + (I_c - I_a)v, \quad \phi^S = \phi_a^S + (\phi_b^S - \phi_a^S)u + (\phi_c^S - \phi_a^S)v. \quad (3.11)$$

The gradient ∇I is given by

$$\nabla I = (I_b - I_a)\nabla u + (I_c - I_a)\nabla v = \left(\frac{I_a \mathbf{r}_{cb} + I_b \mathbf{r}_{ac} + I_c \mathbf{r}_{ba}}{2S} \times \mathbf{n} \right), \quad (3.12)$$

where the normal unit vector \mathbf{n} is defined in terms of the vector product of the triangle edge vectors. A similar relation is valid for $\nabla \phi^S$ too.

Now, the total current density inside the triangle, containing both divergence free and source/sink components, is given by

$$h\mathbf{j} = \frac{I_a \mathbf{r}_{cb} + I_b \mathbf{r}_{ac} + I_c \mathbf{r}_{ba}}{2S} + \bar{\sigma} \left(\frac{\phi_a^S \mathbf{r}_{cb} + \phi_b^S \mathbf{r}_{ac} + \phi_c^S \mathbf{r}_{ba}}{2S} \times \mathbf{n} \right). \quad (3.13)$$

4. Energy principle for the thin wall

The equation (2.2) for ϕ^S , which determines the current in the wall due to current sharing with the plasma can be obtained by minimizing the functional W^S

$$W^S = \int \left\{ \frac{\bar{\sigma}(\nabla \phi^S)^2}{2} - j_{\perp} \phi^S \right\} dS - \frac{1}{2} \oint \phi^S \bar{\sigma} [(\mathbf{n} \times \nabla \phi^S) \cdot d\vec{l}]. \quad (4.1)$$

Here the surface integral dS is taken along the wall surface, while the contour integral $d\vec{l}$ is taken along the edges of the conducting surfaces with the integrand representing the surface current normal to the edges. The contour integral takes into account the external voltage applied to the edges of the wall components and vanishes when there is no source/sink of the current through the edges of the wall surface as happens in typical cases.

For the divergence-free part of the surface current the energy principle can be obtained by multiplying the Faraday law equation (2.3) by \mathbf{i}

$$-\mathbf{i} \frac{\partial \mathbf{A}}{\partial t} - \mathbf{i} \nabla (\phi^E - \phi^S) = \bar{\eta} |\mathbf{i}|^2 \quad (4.2)$$

and integrating it over the wall surface.

$$-\int \mathbf{i} \frac{\partial \mathbf{A}}{\partial t} dS + \oint (\phi^E - \phi^S) [\mathbf{i} \cdot (\mathbf{n} \times d\vec{l})] = \int \bar{\eta} |\mathbf{i}|^2 dS, \quad (4.3)$$

The vector potential consists of the following components

$$\mathbf{A} \equiv \mathbf{A}^I + \mathbf{A}^{ext}, \quad \mathbf{A}^{ext} \equiv \mathbf{A}^{pl} + \mathbf{A}^{coil} + \mathbf{A}^S. \quad (4.4)$$

Here \mathbf{A}^I is the self-field of the current \mathbf{i} , while \mathbf{A}^{ext} is generated by the plasma \mathbf{A}^{pl} , external coils \mathbf{A}^{coil} , and \mathbf{A}^S is created by the source/sink current $-\bar{\sigma} \nabla \phi^S$.

The equation (2.3) for the divergence free part of the surface current $\mathbf{i} = (\nabla I \times \mathbf{n})$ can

be obtained from the following energy functional

$$W^I \equiv \frac{1}{2} \int \left\{ \frac{\partial(\mathbf{i} \cdot \mathbf{A}^I)}{\partial t} + \bar{\eta} |\nabla I|^2 + 2 \left(\mathbf{i} \cdot \frac{\partial \mathbf{A}^{ext}}{\partial t} \right) \right\} dS - \oint (\phi^E - \phi^S) \frac{\partial I}{\partial t} dl. \quad (4.5)$$

The first inductive term in the surface integral represents the change of magnetic energy of the current \mathbf{i} , which in the triangle wall model is given by Eq. (3.13). Its vector potential \mathbf{A}^I (3.1) can be expressed in terms of I using explicit formulas for the triangle representation of the wall. The second term describes resistive losses and the third one represents the excitation of the current by other sources.

In derivation of Eq. (4.5) the term with the time derivative is written in the self-conjugated form by using the equality

$$\left(\frac{\partial \mathbf{i}}{\partial t} \cdot \mathbf{A}^I \right) = \left[\nabla \cdot \left(\frac{\partial \mathbf{B}^I}{\partial t} \times \mathbf{A}^I \right) \right] + \left[\nabla \cdot \left(\frac{\partial \mathbf{A}^I}{\partial t} \times \mathbf{B}^I \right) \right] + \left(\frac{\partial \mathbf{A}^I}{\partial t} \cdot \mathbf{i} \right). \quad (4.6)$$

After integration over entire space the first two terms in the right hand side vanishes, while for the terms containing \mathbf{i} the volume integral is reduced to the integration over wall surface, giving thus

$$\int \left(\mathbf{i} \cdot \frac{\partial \mathbf{A}^I}{\partial t} \right) dS = \int \left(\frac{\partial \mathbf{i}}{\partial t} \cdot \mathbf{A}^I \right) dS = \frac{1}{2} \frac{\partial}{\partial t} \int (\mathbf{i} \cdot \mathbf{A}^I) dS. \quad (4.7)$$

Two energy functionals (4.1) for ϕ^S and (4.5) for I are suitable for implementation into numerical codes and constitute the electromagnetic wall model for the wall touching kink and vertical modes.

5. Matrix circuit equations for triangle wall representation

The substitution of I, ϕ^S as a set of plane functions inside triangles (3.12) is straightforward and leads to the finite element representation of W^I, W^S as quadratic forms for unknowns I, ϕ^S in each vertex.

A similar linear representation (3.12) can be chosen for $j_\perp, \bar{\sigma}$ and $\bar{\eta}$

$$j_\perp = j_a + (j_b - j_a)u + (j_c - j_a)v, \quad (5.1)$$

$$\bar{\sigma} = \bar{\sigma}_a + (\bar{\sigma}_b - \bar{\sigma}_a)u + (\bar{\sigma}_c - \bar{\sigma}_a)v, \quad (5.2)$$

$$\bar{\eta} = \bar{\eta}_a + (\bar{\eta}_b - \bar{\eta}_a)u + (\bar{\eta}_c - \bar{\eta}_a)v. \quad (5.3)$$

Now the elementary integrals, entering the energy principle (4.1) with these representations of $\phi^S, j_\perp, \bar{\sigma}$, can be calculated explicitly as

$$J_u \equiv \frac{1}{S} \int u dS = \frac{2}{D} \int_0^1 u du \int_0^{1-u} D dv = \frac{1}{3}, \quad J_v \equiv \frac{1}{S} \int v dS = \frac{1}{3}, \quad (5.4)$$

$$J_{uu} \equiv \frac{1}{S} \int u^2 dS = \frac{1}{6}, \quad J_{vv} \equiv \frac{1}{S} \int v^2 dS = \frac{1}{6}, \quad J_{uv} \equiv \frac{1}{S} \int uv dS = \frac{1}{12}. \quad (5.5)$$

As a result, the energy functional W^S can be reduced to the following matrix form

$$W^S = \sum_i \left\{ \frac{\bar{\sigma}_a + \bar{\sigma}_b + \bar{\sigma}_c}{3} \cdot \frac{(\phi_a^S \mathbf{r}_{cb} + \phi_b^S \mathbf{r}_{ac} + \phi_c^S \mathbf{r}_{ba})_i^2}{8S_i} - S_i \frac{\phi_a^S (2j_a + j_b + j_c) + \phi_b^S (j_a + 2j_b + j_c) + \phi_c^S (j_a + j_b + 2j_c)}{12} \Big|_i \right\}, \quad (5.6)$$

where summation is performed over all triangles. We dropped the contour integral term which is zero for most of plasma dynamics problems.

In the energy functional W^I the vector potential \mathbf{A}^I is generated by the surface currents from the entire wall

$$\mathbf{A}^I(\mathbf{r}) \equiv \sum_j \mathbf{i}_j \varphi_j(\mathbf{r}), \quad \frac{\partial \mathbf{A}^I(\mathbf{r})}{\partial t} = \sum_j \frac{(\dot{I}_a \mathbf{r}_{cb} + \dot{I}_b \mathbf{r}_{ac} + \dot{I}_c \mathbf{r}_{ba})_j}{2S_j} \varphi_j(\mathbf{r}), \quad (5.7)$$

where the dot stands for the time derivative $\dot{I} = dI/dt$. In the energy integral each j -term in this sum should be integrated over each i -triangle of the wall. The following notation is introduced for the elementary integrals representing the mutual capacitance of two triangles

$$C_{ij} = C_{ji} \equiv \int dS_i \int \frac{dS_j}{|\mathbf{r}_i - \mathbf{r}_j|}. \quad (5.8)$$

They have to be evaluated numerically. Other terms in W^I can be expressed in the same way as in the previous case of the W^S functional.

As a result, W^I acquires the following quadratic form representation

$$\begin{aligned} W^I = & \frac{d}{dt} \left\{ \sum_{ij} C_{ij} \frac{[(I_a \mathbf{r}_{cb} + I_b \mathbf{r}_{ac} + I_c \mathbf{r}_{ba})_i \cdot (I_a \mathbf{r}_{cb} + I_b \mathbf{r}_{ac} + I_c \mathbf{r}_{ba})_j]}{8S_i S_j} \right\} \\ & + \sum_i \left\{ S_i \langle \bar{\eta} \rangle_i \cdot \frac{g_{uu}(I_b - I_a)^2 + 2g_{uv}(I_b - I_a)(I_c - I_a) + g_{vv}(I_c - I_a)^2}{2} \right\} \\ & + \sum_i \left\{ \frac{[(I_a \mathbf{r}_{cb} + I_b \mathbf{r}_{ac} + I_c \mathbf{r}_{ba})_i \cdot \langle \dot{\mathbf{A}}^{ext} \rangle_i]}{2S_i} \right\}, \end{aligned} \quad (5.9)$$

with

$$\langle \bar{\eta} \rangle_i \equiv \frac{\bar{\eta}_a + \bar{\eta}_b + \bar{\eta}_c}{3}, \quad \langle \dot{\mathbf{A}}^{ext} \rangle_i \equiv \frac{\dot{\mathbf{A}}_a^{ext} + \dot{\mathbf{A}}_b^{ext} + \dot{\mathbf{A}}_c^{ext}}{3}.$$

Here, the dot at $\dot{\mathbf{A}}^{ext}$ stands for the time derivative.

The minimization of quadratic forms (5.6,5.9) leads to linear systems of equations with symmetric positively defined matrices which can be solved using the Cholesky decomposition.

6. Simulations of Source/Sink Currents using SSC code

In accordance with the two types of wall currents two numerical codes are presented. The shell simulation code SHL implements the matrix equations, resulted from W^I Eq. (5.9), and solves them with given right hand side $\dot{\mathbf{A}}^{ext}$ in Eq. (5.9). The S/S current simulation code SSC complements SHL by calculation of S/S-currents in the wall with given right hand side j_\perp in Eq.(5.6).

The wall in both codes is represented as a structure

```
<Body>[nS]{
<Surface 0>;
<Surface 1>;
.....
```

```
<Surface nS-1>;
}
```

At this moment, by definition there is no electric current sharing between different surfaces across the gaps or along the third dimension (such as grounding). For convenience, the surfaces are enclosed into <Body> structures. In future, the electric connection between surfaces can be implemented as another j_{\perp} effect.

Each surface consists of a number of vertexes and triangles and can contain a single closed edge and potentially multiple holes. The I and ϕ^S functions on different surfaces are independent, with $I = 0$ along the edges, or at a single point, if edges are absent (as for a toroidal shell). Along the edges of the holes $I = \text{const}$ with values determined by equations. Similarly, the function ϕ^S is specified at one of the vertexes.

Fig. 2 shows an example of calculations of the source/sink currents on a toroidal shell Fig. 2a with a set vertical and horizontal holes. In this example, the wall surface does not contain the edge.

Two localized source (red) and sink (blue) areas are prescribed as shown in Fig. 2b and the wall conductivity $\bar{\sigma}$ is assumed to be constant and equal to 1 for simplicity. The distribution of the solution $\bar{\sigma}\phi^S$ of Eq. (2.2) over the wall surface (outside the source/sink area) is shown in Figs. 2c,d. The color reflects its amplitude in accordance with the color rule at the right side of the frame. Short straight lines indicate the vectors of the current density $-\bar{\sigma}\nabla\phi^S$ with the length proportional to its local amplitude with a dot at the beginning of the vector. The surface currents are concentrated predominantly between source and sink.

7. Verification of SSC with an analytical solution

The accuracy of the SSC code was checked against the following analytical example. For simplicity, we consider $\bar{\sigma} = 1$ and a toroidal shell, which is shown in Fig. 3 and defined in Cartesian coordinates x, y, z by

$$x = (R - a \cos \omega) \cos \varphi, \quad y = (R - a \cos \omega) \sin \varphi, \quad z = a \sin \omega, \quad (7.1)$$

where φ, ω are poloidal and toroidal angles and R, a are the major and minor radii. The poloidal and toroidal cuts are defined by

$$\varphi_0 = \epsilon \leq \varphi \leq 2\pi - \epsilon = \varphi_3, \quad \omega_0 = \epsilon \leq \omega \leq 2\pi - \epsilon = \omega_3, \quad \epsilon = 0.01, \quad (7.2)$$

The hole area is symmetric with respect to the point $\varphi = \pi, \omega = \pi$ and is specified by

$$u \equiv \varphi - \pi, \quad v \equiv \omega - \pi, \quad |u| \leq u_0 = \frac{\pi}{4}, \quad |v| \leq v_0 = \frac{\pi}{4}. \quad (7.3)$$

The analytical solution is chosen in the form

$$\phi^S = \int_0^u G_u(u) du \cdot \int_0^v G_v(v) dv \quad (7.4)$$

with

$$G_u(u_0) = G_u(-u_0) = G_u(u_1) = G_u(-u_1) = G_v(v_0) = G_v(-v_0) = G_v(v_1) = G_v(-v_1) = 0, \quad (7.5)$$

$$u_1 = v_1 = \pi - \epsilon$$

to satisfy the absence of the current flow through the edges of the shell. One specific choice is given by

$$G_u(u) = (u^2 - u_0^2)(u^2 - u_1^2), \quad G_v(v) = (v^2 - v_0^2)(v^2 - v_1^2). \quad (7.6)$$

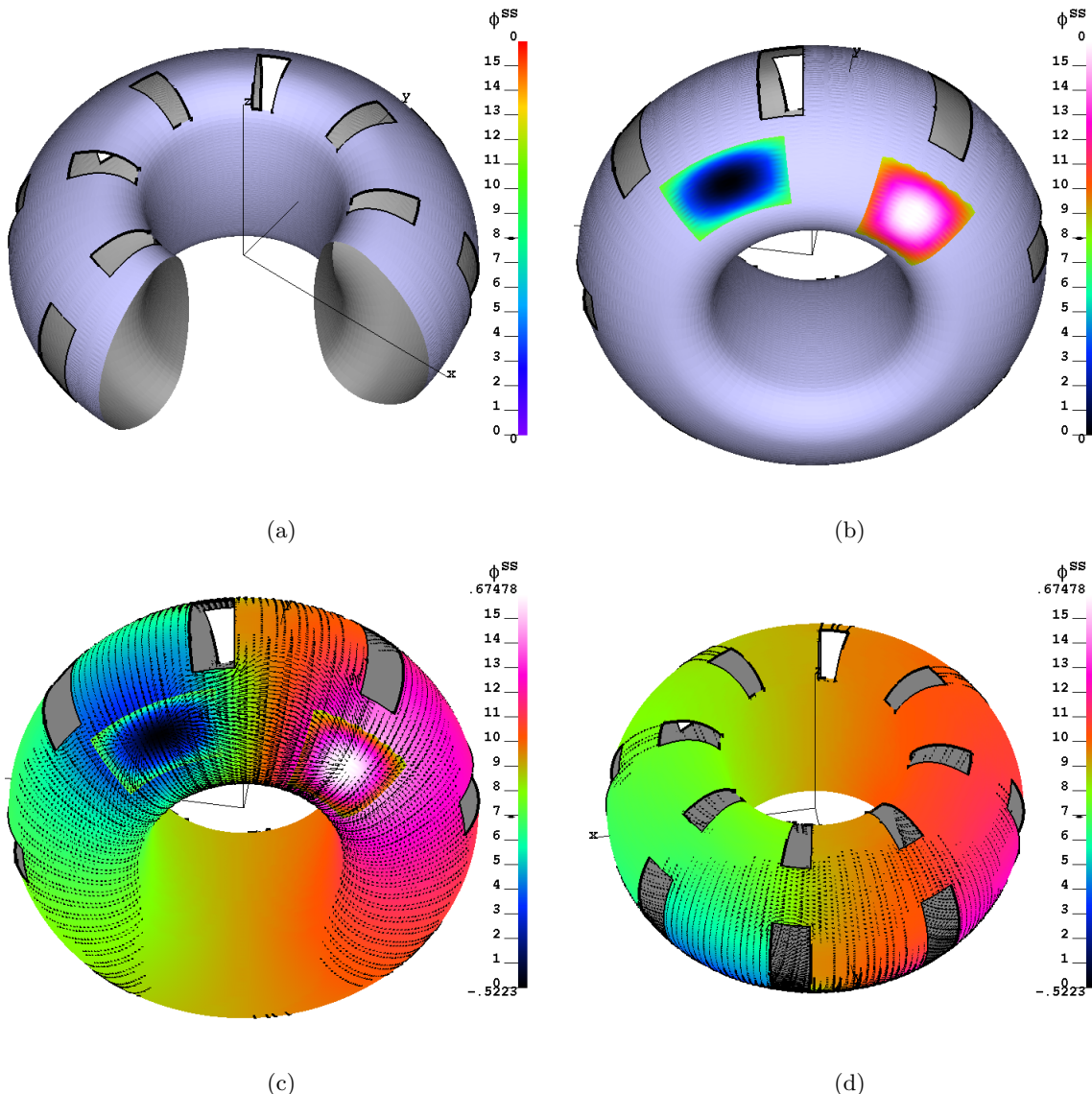


FIGURE 2. SSC simulations of source/sink currents on a toroidal shell with holes and localized wetting zones. (a) Toroidal thin wall with holes. (b) Wetting zones with distributed j_{\perp} . (c) View to the bottom of the wall on distribution of the solution ϕ^S . (d) View to the top where the S/S-currents are small. White and black ends of the color map correspond to positive and negative values correspondingly.

The source term j_{\perp} for the SSC code can be calculated in a straightforward way with the following relation

$$j_{\perp} = -\Delta\phi^S = -\frac{1}{a(R - a \cos \omega)} \left[\frac{a}{R - a \cos \omega} \frac{\partial^2 \phi^S}{\partial \varphi^2} + \frac{\partial}{\partial \omega} \left(\frac{R - a \cos \omega}{a} \frac{\partial \phi^S}{\partial \omega} \right) \right] \quad (7.7)$$

and is shown in Fig. 3b.

Figs. 3c,3d illustrate the comparison of the analytical and numerical solutions for dif-

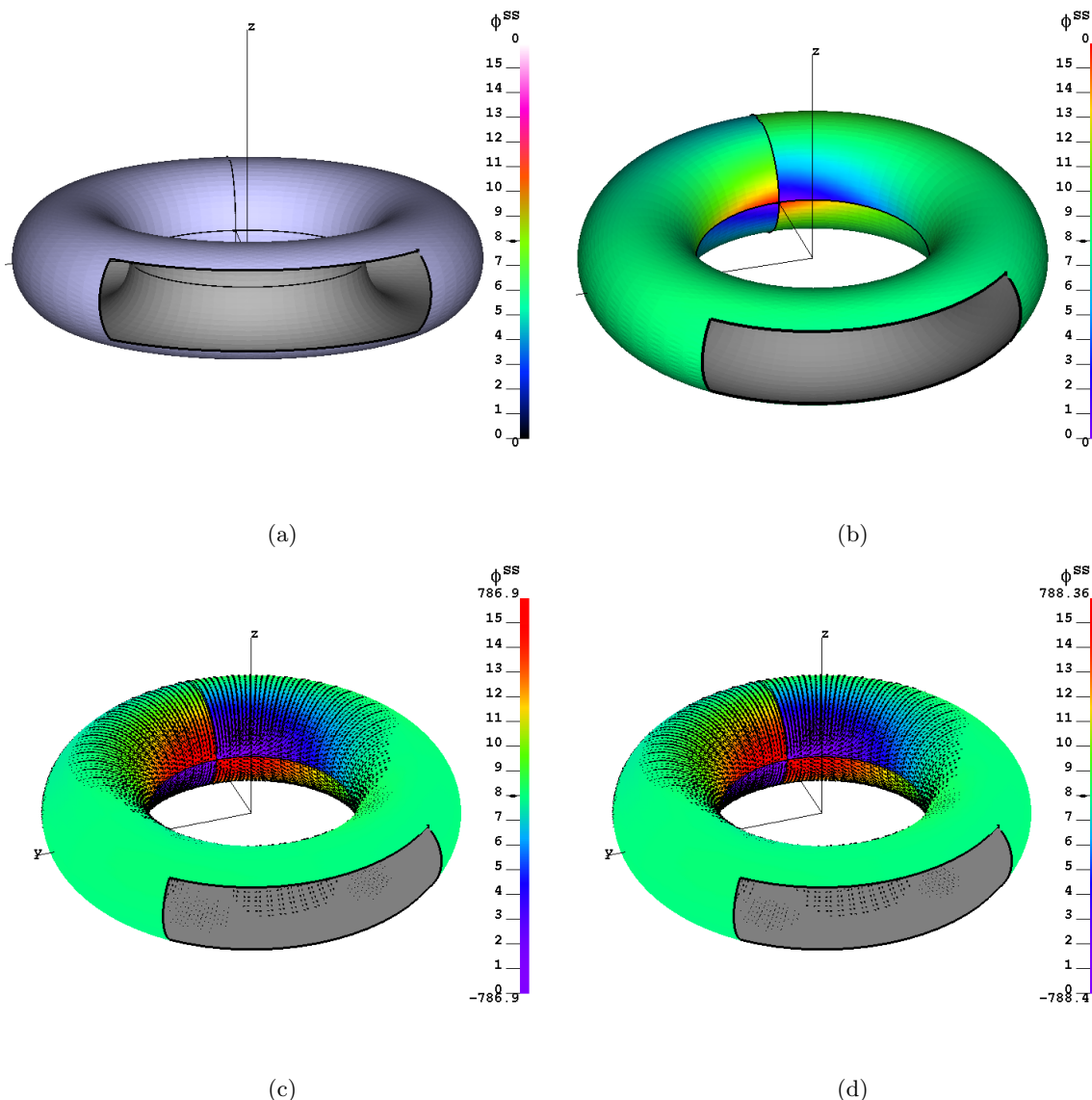


FIGURE 3. High resolution model (64x64x4 triangles) of a wall (the major/minor radii are 3/1). (a) a wall with a poloidal and toroidal cuts and a hole in the low field side surface. (b) Color image of the input j_{\perp} . (c) Color image of the analytical ϕ^S . Straight lines show the direction of the current density with a point labeling the beginning of the vector. (d) The same based on numerical solution. The value of the relative inaccuracy is 0.001.

ferent triangularizations of a toroidal shell. The high resolution mesh (64x64x4 triangles) on the wall surface was used in Fig. 3d, providing a relative accuracy of 0.001.

Figs. 4,5 represent the same calculations with a medium (32x32x4) and rough (16x15x4) resolution which provide the relative accuracy 0.003 and 0.015 respectively.

These numbers show that the grid representation of the wall does not represent an issue for disruption simulations.

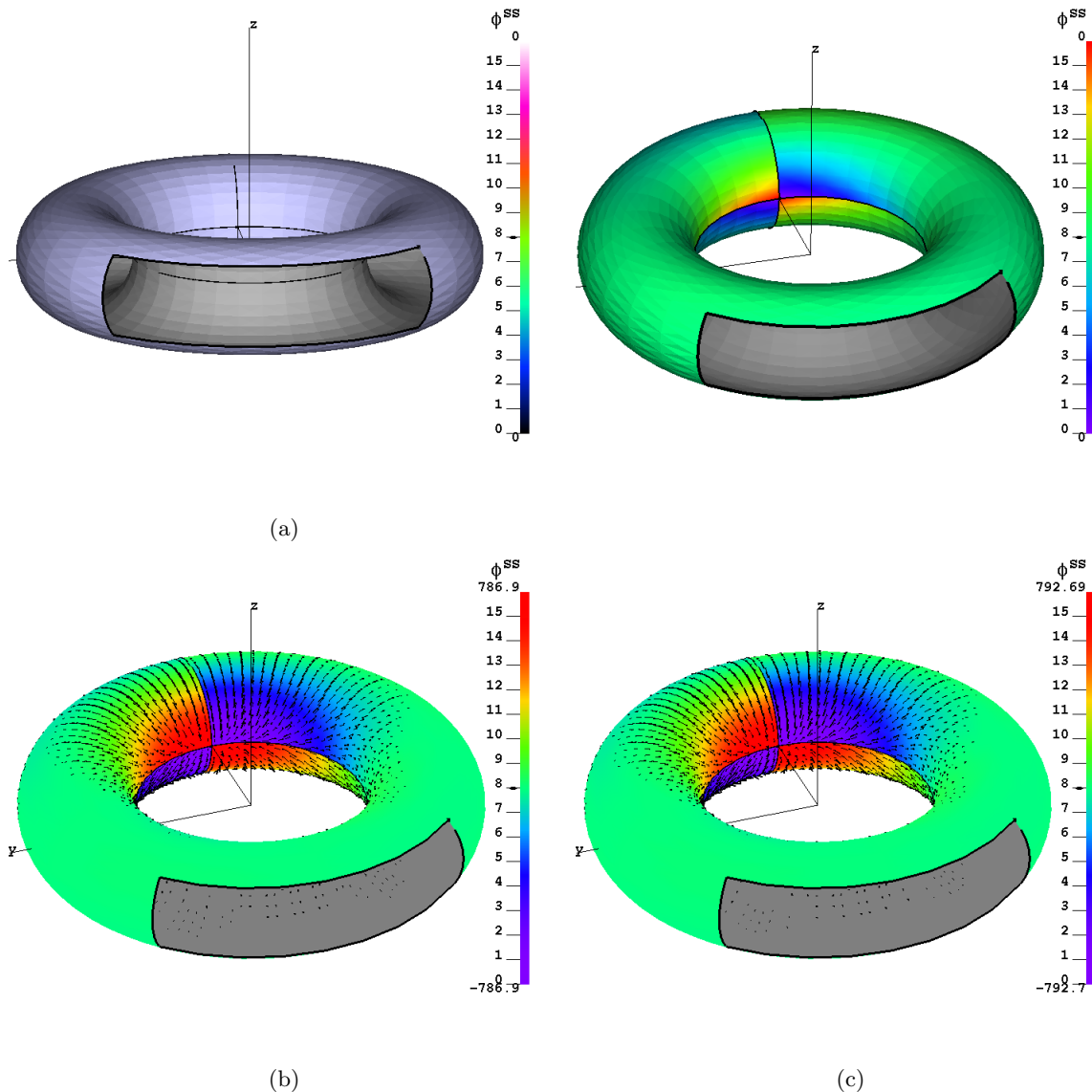


FIGURE 4. (a) Medium resolution triangle model of a wall (the major/minor radii are 3/1). (b) Color image of the input j_{\perp} . (c) Color image of the analytical ϕ^S . Straight lines show the direction of the current density with a point labeling the beginning of the vector. (d) The same based on numerical solution. The value of the relative inaccuracy is 0.003.

8. A step toward modeling the Wall Touching Kink Modes

This section describes the initial steps in simulation of the Hiro and eddy currents excitation in the wall by mutually interfaced SSC and SHL codes. The plasma kink deformation and vertical displacement are prescribed and a circular plasma cross-section is considered for simplicity. The strong toroidal magnetic field approximation was also used for the surface currents calculation at the plasma edge as in Ref. (Zakharov 2008). The wetting zone is determined by the intersection of plasma and wall surfaces. In a real situation, it should be determined in a self-consistent manner by the 3-D equilibrium

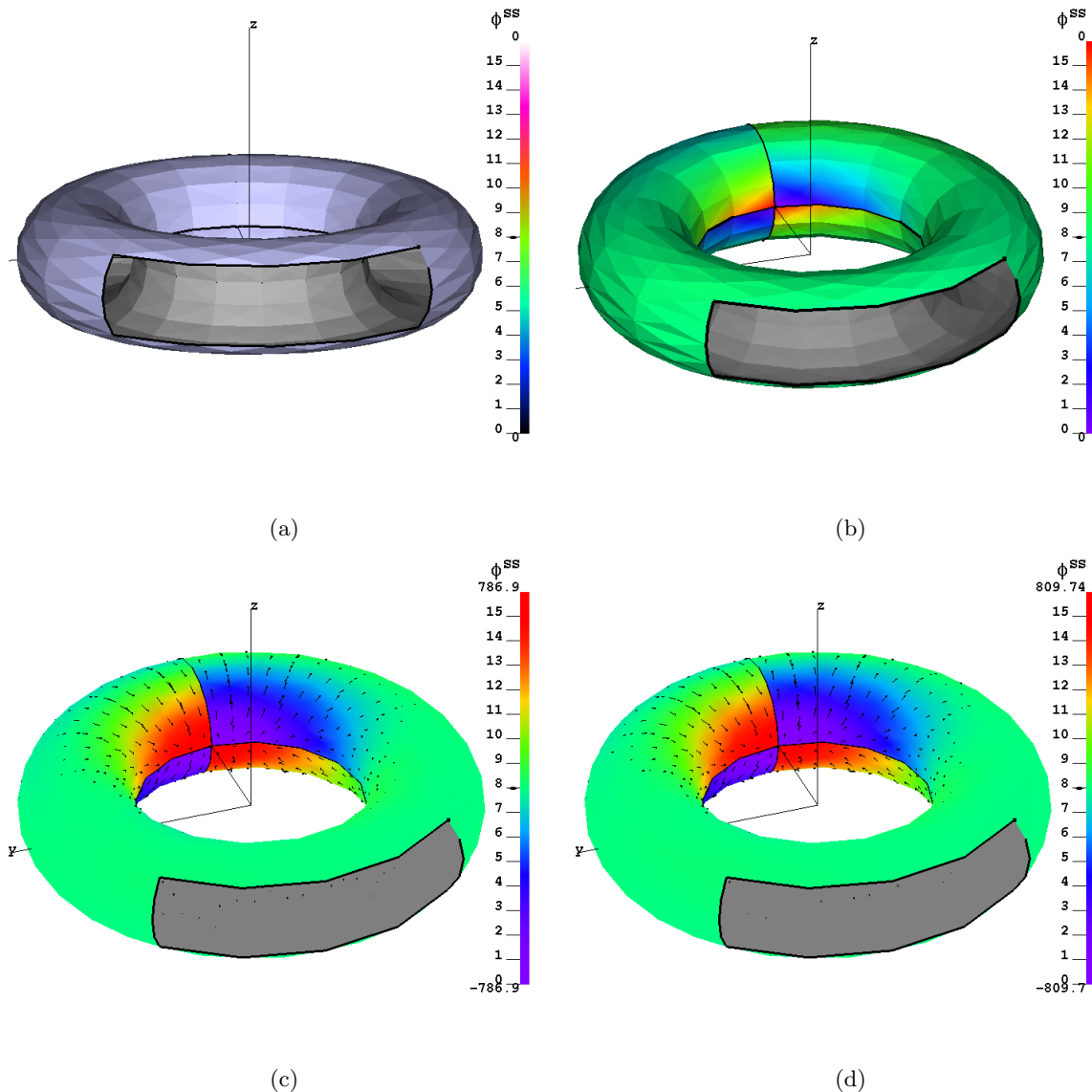


FIGURE 5. (a) Low resolution triangle model of a wall (the major/minor radii are 3/1). (b) Color image of the input j_{\perp} . (c) Color image of the analytical ϕ^S . Straight lines show the direction of the current density with a point labeling the beginning of the vector. (d) The same based on numerical solution. The value of the relative inaccuracy is 0.015.

equation of TMHD together with the plasma shape and position. The j_{\perp} -profile is prescribed now in a simplified manner as a source/sink distributed over the wetting zone. Its amplitude is consistent with the current sharing with the plasma edge. In reality, j_{\perp} -profile should be determined by the structure of DSoL of Hiro currents. The Evans currents are neglected. The resistivity of the wall was also neglected in Faraday's law (2.3).

With these assumptions, the S/S-current is calculated by the SSC code. In turn, the SHL code calculates the eddy currents in the wall generated by the plasma kink deformation and by S/S-current. All together they represent the total surface current in

the wall. What is missed at this stage of the code development is the backward effect of these currents on the plasma shape and its surface currents. This important and complicated step is left for a future development.

Figs. 6,7 show the calculations which mimic the wetting zone and Hiro currents due to Wall Touching Kink Mode during an AVDE. Fig. 6b shows a toroidal plasma, shifted upward and perturbed by a $m/n = 1/1$ kink perturbation. As a result, a wetting zone is created and displayed as a piece of plasma surface in front of the inner wall. The blue color on the plasma surface indicates the direction of the surface current, opposite to the plasma current, while the red color corresponds to the plasma surface currents in the same direction as the plasma current.

It is a fundamental result of the theory of the wall touching modes (Zakharov 2008; Zakharov *et al.* 2012) that the Hiro currents are negative (relative to the total plasma current). They determine the sign the source j_{\perp} for S/S-currents as it is reflected in Fig. 6c by color of the wetting zone (red for positive and blue for the negative j_{\perp}). For exemplification only, j_{\perp} is prescribed as uniform in the vertical direction with the amplitude corresponding to the Hiro current entering the wetting zone at a particular azimuth, as shown in Fig. 6c by colors in the wetting zone. Fig. 6d presents the solution to Eq. (2.2). Four frames in Fig. 7 show different views on the solution ϕ^S and the pattern of the S/S current density represented by the short straight lines. All calculations (35840 triangles in this case) are made on a single processor mode on M3800 Dell laptop and take several seconds to calculate ϕ^S (if the Cholesky decomposed matrix is given). The significant reserve in the code acceleration by using the cyclic matrix Fourier decomposition of Graphic Processor Units was not yet used.

Four frames of Fig. 8 show the results of combined calculations by the SSC and SHL of the S/S and eddy currents in the wall. The color of the wall surface in Fig. 8a displays the amplitude of the toroidal component of the vector potential A_{φ}^{pl} of the plasma magnetic perturbation. The eddy current i^{pl} due to the “ideal” response of the wall to the plasma perturbed magnetic field is shown in Fig. 8b. The color of the wall surface reflects the value of the stream function I of the eddy currents. Fig. 8c displays the eddy current i^S excited by the S/S-current, while the surface color represents ϕ^S as in Fig. 6d.

The final Fig. 8d shows the total surface current, which includes both above mentioned eddy currents and the S/S-current. The color of the surface is the same as in Fig. 8c. It appears to be an important result of the present calculations that the total surface current is dominated by the S/S-current due to sharing of Hiro currents with the plasma. Thus, the relative average amplitudes of eddy currents relative to S/S current are given by

$$\frac{\sqrt{\int |\nabla\phi^S|^2 dS}}{\sqrt{\int i^{2pl} dS}} = 44.5, \quad \frac{\sqrt{\int |\nabla\phi^S|^2 dS}}{\sqrt{\int i^{2S} dS}} = 2.41, \quad (8.1)$$

where the integration is over the wall surface.

These numbers reflect the fundamental physics of the WTKM (Zakharov *et al.* 2012). The Hiro currents for the $m/n = 1/1$ kink mode are not sensitive to the edge value of the safety factor q_a and for circular plasma with major and minor radii R, a are given simply by

$$\mu_0 \mathbf{i}^{Hiro} = -2 \frac{B_{\varphi}}{R} \xi \left(1 - \frac{1 - q_a}{q_a} \lambda \right) \left(\mathbf{e}_{\varphi} + \frac{a}{R} \mathbf{e}_{\omega} \right) \cos(\omega - \varphi), \quad (8.2)$$

where \mathbf{e}_{ω} is the poloidal unit vector on the plasma surface. The factor $\lambda < 1$ in the second non-significant term takes into account the effect of the wall. In present simulations

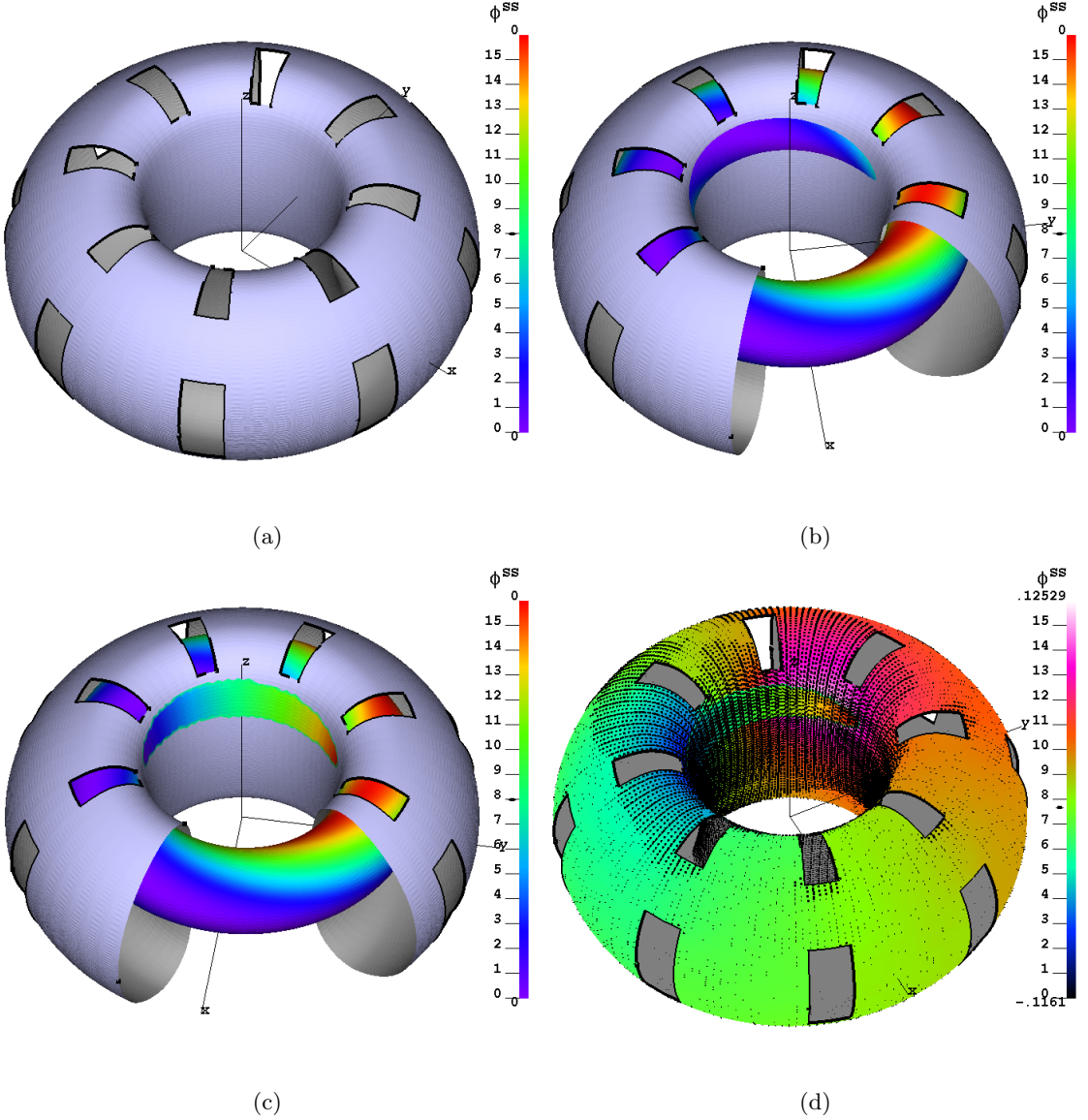


FIGURE 6. S/S-currents in a toroidal shell represented by 140×64 quads with 4 triangles inside each. (a) The toroidal thin wall shell with multiple holes. (b) A toroidal plasma shifted vertically with a $m/n = 1/1$ kink deformation. The colors of the plasma surface corresponds the direction of surface currents: blue for the opposite and red for the same direction as the plasma current. (c) Wetting zones due to Wall Touching Kink Mode and the color representation of j_{\perp} ; (d) The resulting ϕ^S and vectors of the current density.

$q_a = 0.9$, as it could be realistically expected for the experimental situation in AVDEs. For any q_a near the resonant level, \mathbf{i}^{Hiro} are essentially determined by the first term of the equation.

At the same time, the magnetic field perturbation outside the plasma is proportional

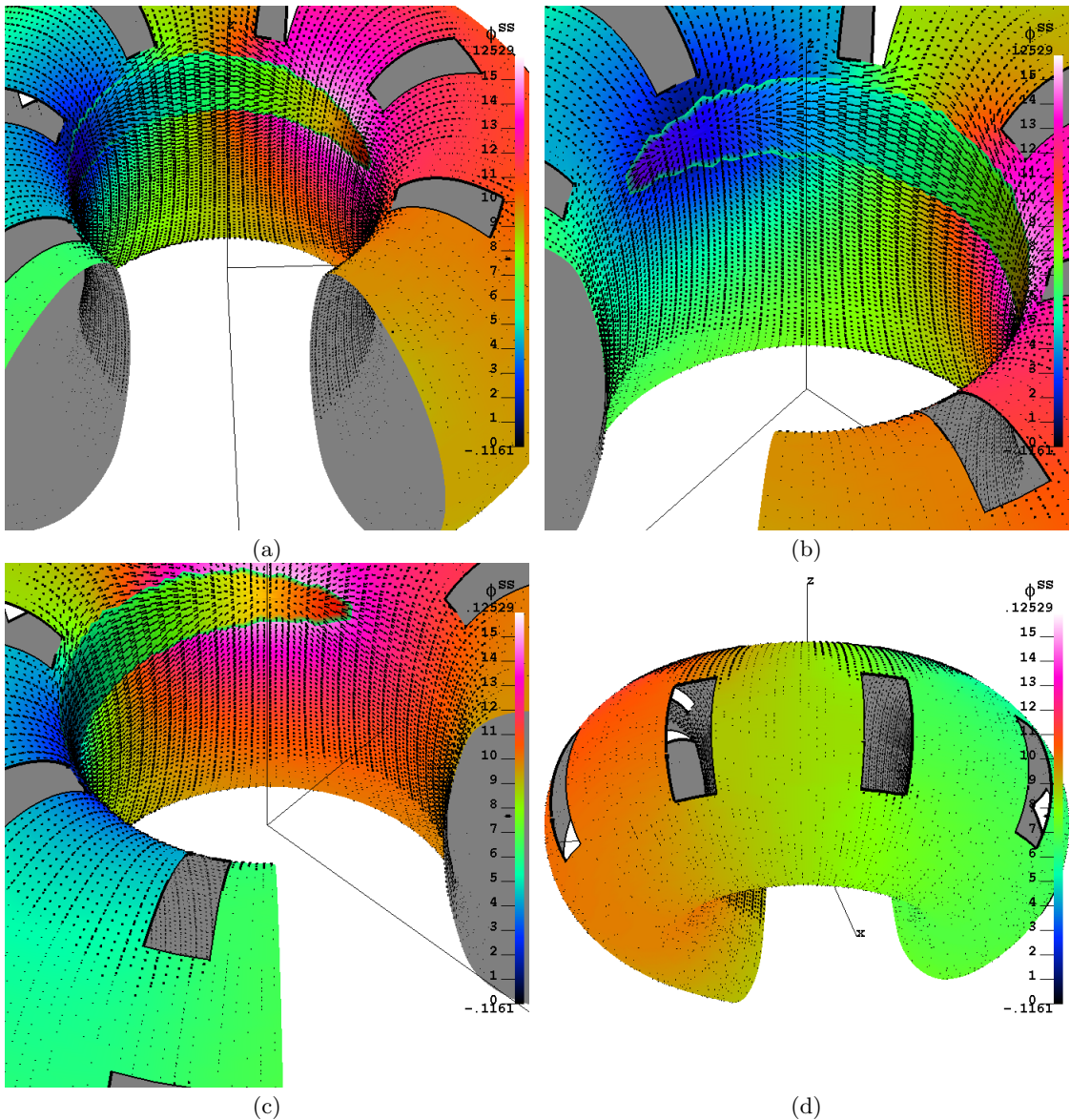


FIGURE 7. Color representation of the resulting ϕ^S and S/S-currents $-\bar{\sigma}\nabla\phi^S$. (a) The zoomed view on the wetting zone which contains the major part of the S/S-current. (b) The zoomed view on the sink zone with S/S currents converging to its center. (c) The zoomed view on the source zone with S/S currents diverging from its center. (d) Bottom view, showing the lack of the S/S-currents at the bottom part of the wall.

to the resonant factor $(1 - q_a)$

$$rA_\varphi = \frac{a^2}{R\rho}\xi B_\varphi \frac{1 - q_a}{q_a} \cos(\theta - \varphi), \quad (8.3)$$

where ρ is the polar radius counted from the plasma axis at $\varphi = \text{const}$.

This difference in amplitude explains the dominant role of S/S-currents excited by Hiro currents in the wetting zone of the wall. The opposite direction with respect to the

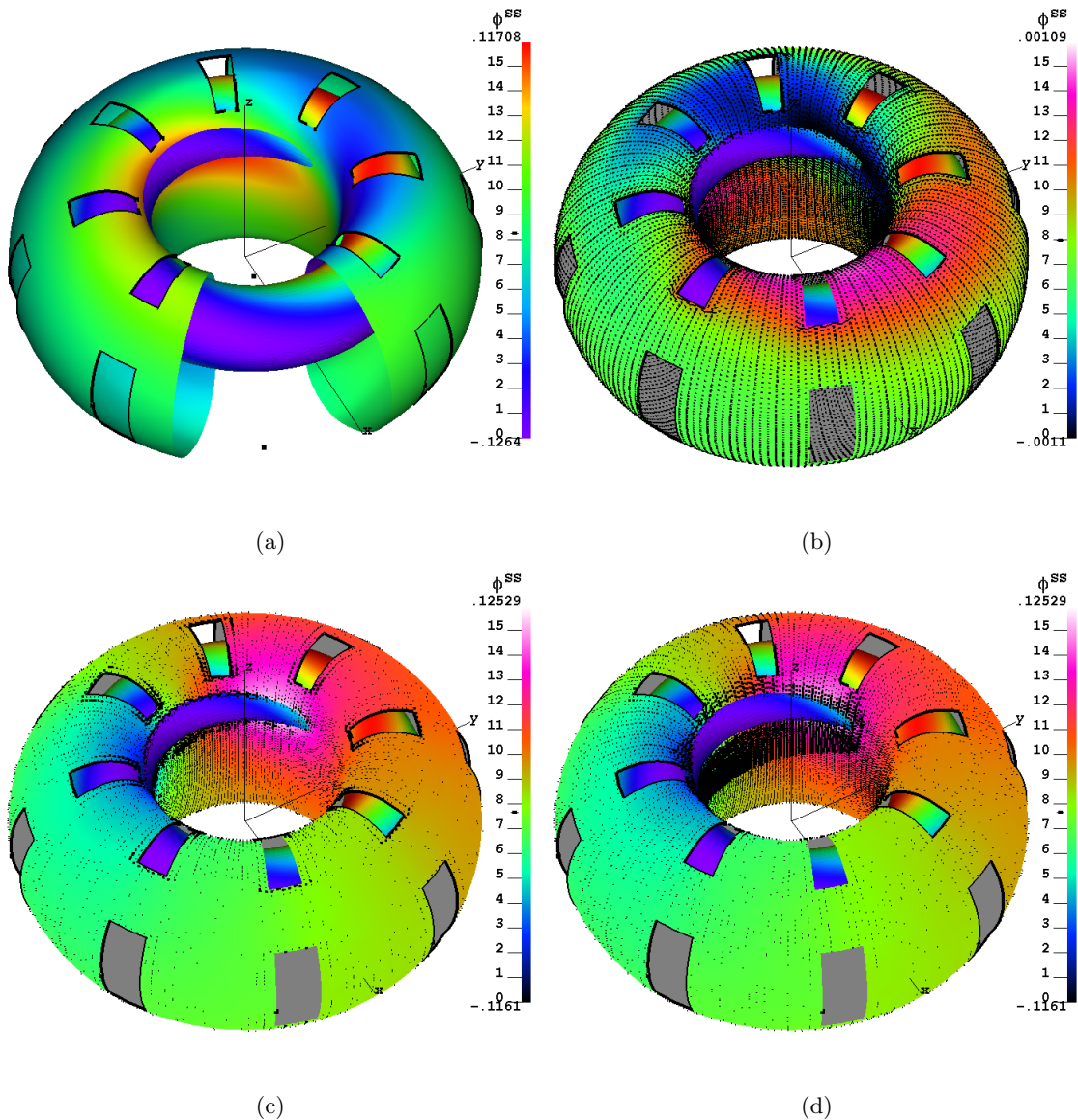


FIGURE 8. S/S-currents in a toroidal shell represented by 140×64 quads with 4 triangles inside each. (a) toroidal thin wall shell with multiple holes and a plasma inside. (b) Wetting zones due to Wall Touching Kink Mode. (c) Representation of j_{\perp} on triangular grid (d) resulting ϕ^S and vectors of the current density.

plasma current direction can explain the negative loop voltage spike appearing when the plasma touches the wall at the beginning of the disruptions.

9. Optimization of the solutions to the source/sink equation

As in the previous examples, given the source term j_{\perp} , the Eq. (2.2) for the source/sink current can be solved in the entire domain separately from Eq. (2.4). At the same time, the representation of the source/sink current in terms of a source potential $-\bar{\sigma} \nabla \phi^S$ is

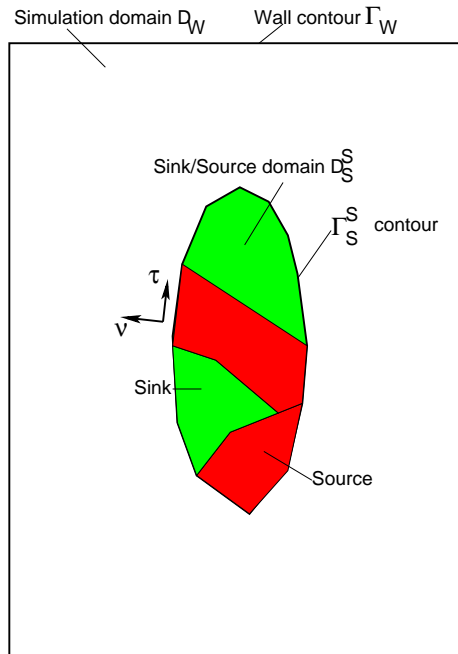


FIGURE 9. A single connected domain D_S^S , limited by a contour Γ_S^S with the source/sink current j_\perp inside.

essential only in the domain containing j_\perp . Outside it, the surface current is divergence-free and both representations are valid. In particular, the uniform current density in a single triangle can be represented by

$$\mathbf{i} = \frac{I_a \mathbf{r}_{cb} + I_b \mathbf{r}_{ac} + I_c \mathbf{r}_{ba}}{2S} = \langle \bar{\sigma} \rangle \left(\frac{\phi_a^S \mathbf{r}_{cb} + \phi_b^S \mathbf{r}_{ac} + \phi_c^S \mathbf{r}_{ba}}{2S} \times \mathbf{n} \right). \quad (9.1)$$

The relations between the stream function I and gradient ϕ^S representations are given by

$$I_b - I_a = (\phi_b^S - \phi_a^S) \frac{(\mathbf{r}_{ba} \cdot \mathbf{r}_{ac})}{4S^2} (\phi_c^S - \phi_a^S) \frac{(\mathbf{r}_{ba} \cdot \mathbf{r}_{ba})}{4S^2}, \quad (9.2)$$

$$I_c - I_a = -(\phi_b^S - \phi_a^S) \frac{(\mathbf{r}_{ac} \cdot \mathbf{r}_{ac})}{4S^2} - (\phi_c^S - \phi_a^S) \frac{(\mathbf{r}_{ba} \cdot \mathbf{r}_{ac})}{4S^2}. \quad (9.3)$$

For both I and φ^S , the additive constants are not important and for a separate triangle $I_a = 0$ and $\phi_a^S = 0$ can be considered.

This dual representation opens an opportunity to solve the problem with the maximum use of the divergence-free representation of the surface current.

In this section we consider two cases: a single domain, containing both source and sink area, and two separated domains with a source and a sink area. The calculations in the previous sections give the examples of both cases.

9.1. Single domain with source and sink inside

The simplified sketch of the domain topology is given in Fig. 9

$$\int_{D_S^S} j_\perp dS = 0. \quad (9.4)$$

Vectors $\vec{\tau}, \vec{\nu}$ are the unit vectors tangential and normal to Γ_S^S , respectively

$$(\vec{\nu} \times \vec{\tau}) = \mathbf{n}. \quad (9.5)$$

Inside Γ_S^S the surface current density is represented by

$$h\mathbf{j}_S^S = -\bar{\sigma}\nabla\phi^S \quad (9.6)$$

and outside it

$$h\mathbf{j}_S^S = (\nabla I_S^S \times \mathbf{n}) \quad (9.7)$$

In this case, Eq. (2.2) for the source potential ϕ^S should be solved inside the D_S^S domain

$$(\nabla \cdot (\bar{\sigma}\nabla\phi^S))|_{D_S^S} = -j_\perp. \quad (9.8)$$

Outside it (between Γ_S^S and the wall contour Γ_W), a stream function representation of the source/sink current is valid as well

$$-\bar{\sigma}\nabla\phi^S \equiv (\nabla I_S^S \times \mathbf{n}), \quad (\nabla \cdot (\bar{\eta}\nabla I_S^S)) = 0 \quad (9.9)$$

with the mixed Dirichlet-Neumann boundary conditions at Γ_S^S , expressing the continuity of the current $h\mathbf{j}$ density at Γ_S^S , and the Dirichlet condition at Γ_W

$$\bar{\sigma}(\vec{\nu} \cdot \nabla\phi^S)|_{\Gamma_S^S} = -(\vec{\tau} \cdot \nabla I_S^S)|_{\Gamma_S^S}, \quad (9.10)$$

$$\bar{\sigma}(\vec{\tau} \cdot \nabla\phi^S)|_{\Gamma_S^S} = (\vec{\nu} \cdot \nabla I_S^S)|_{\Gamma_S^S}, \quad (9.11)$$

$$I_S^S|_{\Gamma_W} = 0. \quad (9.12)$$

This combined solution gives the solution for the Eq. (2.2) in the entire domain.

Next, the contribution of the S/S-current $h\mathbf{j}_S^S$ to Eq. (2.4) (or to its variational form) can be calculated using Bio-Savart formulas, and then the Eq. (2.4) solved in the entire wall domain.

As a result, the total surface current density will be given by

$$h\mathbf{j} = \begin{cases} (\nabla I \times \mathbf{n}) - \bar{\sigma}\nabla\phi^S & \text{inside } D_S^S, \\ (\nabla I \times \mathbf{n}) + (\nabla I_S^S \times \mathbf{n}) & \text{between } \Gamma_S^S \text{ and } \Gamma_W. \end{cases} \quad (9.13)$$

9.2. Two separated domains with sources/sinks

Fig.10 gives a simplified sketch of two domains. In the following notations, the superscript corresponds to the source and the subscript corresponds to the sink domain.

$$\int_{D^S} j_\perp dS = I^S \neq 0, \quad (9.14)$$

$$\int_{D^S} j_\perp dS = -I^S \neq 0, \quad (9.15)$$

$$\int_{D^S} j_\perp dS + \int_{D^S} j_\perp dS = 0 \quad (9.16)$$

Vectors $\vec{\tau}_S, \vec{\nu}_S, \vec{\tau}^S, \vec{\nu}^S$ are the unit vectors tangential and normal to Γ_S, Γ^S , respectively.

In this case there is a non-zero current flow I^S from D^S to D_S and a cut between the two domains is necessary to represent the divergence free current $(\nabla I_S^S \times \mathbf{n})$ outside D_S, D^S . At the sides of the cut, its values I_C, I^C are different

$$I_C = I^C + I^S. \quad (9.17)$$

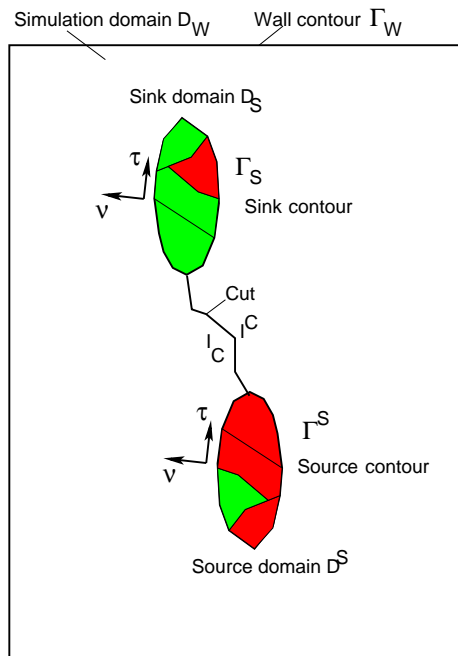


FIGURE 10. Separate sink D_S and source D^S domains, limited by the contours Γ_S and Γ^S with j_\perp inside.

Otherwise, a similar problem with Eq.(2.2) inside the domains D_S, D^S for ϕ^S and Eq.(9.9) for I_S^S outside it and with mixed boundary conditions at Γ^S, Γ_S should be solved as in the previous case.

9.3. A unified formulation for the surface currents

For practical implementation I_S^S can be consumed by the stream function I , which is discontinuous (double-valued at Γ_S^S) together with its normal derivative ($\vec{\nu} \cdot \nabla I$) across Γ_S^S . Using 'e,i' superscripts in order to specify the external and internal values of discontinuous functions at the contour Γ_S^S , we denote the two values of I at Γ_S^S by I^e, I^i .

The system of equations for the surface current can be written as a system of Eqs.(2.2,2.4)

$$(\nabla \cdot (h\mathbf{j})) = -(\nabla \cdot (\bar{\sigma} \nabla \phi^S)) = -j_\perp \quad \text{inside } D_S^S, \quad (9.18)$$

$$(\nabla \cdot (\bar{\eta} \nabla I)) = \frac{\partial(B_\perp^I + B_\perp^S)}{\partial t} + \frac{\partial(B_\perp^{pl} + B_\perp^{coil})}{\partial t} \quad \text{inside } \Gamma_W, \text{ excluding the contour } \Gamma_S^S \quad (9.19)$$

with mixed Dirichlet-Neumann boundary conditions at the source/sink contour Γ_S^S and the Dirichlet condition at the wall contour Γ_W

$$\bar{\sigma}(\vec{\nu} \cdot \nabla \phi^S) = -[\vec{\tau} \cdot \nabla(I^e - I^i)] \quad \text{at } \Gamma_S^S, \quad (9.20)$$

$$\bar{\sigma}(\vec{\tau} \cdot \nabla \phi^S) = (\vec{\nu} \cdot \nabla I)^e - (\vec{\nu} \cdot \nabla I)^i \quad \text{at } \Gamma_S^S, \quad (9.21)$$

$$I = 0 \quad \text{at } \Gamma_W. \quad (9.22)$$

The resulting total surface current density is given by

$$h\mathbf{j} = (\nabla I \times \mathbf{n}) + \begin{cases} -\bar{\sigma} \nabla \phi^S & \text{inside } D_S^S, \\ 0 & \text{between } \Gamma_S^S \text{ and } \Gamma_W. \end{cases} \quad (9.23)$$

The same problem can be formulated in terms of the following variational principle

$$\frac{\partial W_S^S}{\partial \phi^S} = 0, \quad \frac{\partial W^I}{\partial I} = 0, \quad (9.24)$$

where

$$W^I \equiv \int_{D_w} \left\{ \frac{\partial((\nabla I \times \mathbf{n}) \cdot (\mathbf{A}^{I+S}))}{2\partial t} + \bar{\eta} \frac{|(\nabla I \times \mathbf{n})|^2}{2} + \left((\nabla I \times \mathbf{n}) \cdot \frac{\partial \mathbf{A}^{pl+coil}}{\partial t} \right) \right\} dS \\ + \oint_{\Gamma_S^S} (I^e - I^i)(\vec{\tau} \cdot \nabla \phi^S) dl, \quad (9.25)$$

$$W_S^S \equiv \int_{D_S^S} \left\{ \frac{\bar{\sigma}(\nabla \phi^S)^2}{2} - j_{\perp} \phi^S \right\} dS + \oint_{\Gamma_S^S} \phi^S (\vec{\tau} \cdot \nabla I) dl, \quad (9.26)$$

$$\mathbf{A}^{I+S}(\mathbf{r}) \equiv \int_{D_w} \frac{(\nabla I \times \mathbf{n}) - \bar{\sigma} \nabla \phi^S}{|\mathbf{r} - \mathbf{r}'|} dS'. \quad (9.27)$$

10. Summary

The rigorous mathematical formulation of the surface current circuit equations for the thin wall is formulated. In the triangular representation of the wall surface, both divergence-free eddy and source/sink currents are represented by the same model of a uniform current density inside each triangle. This model is implemented in the source/sink code SSC and the shell simulation code SHL.

The coupling of finite element matrix equations for both types of currents contains the same matrix elements of mutual capacitance C_{ij} of two triangles $\{i, j\}$

$$C_{ij} \equiv \int_{\Delta_i} \int_{\Delta_j} \frac{dS_i dS_j}{|\mathbf{r} - \mathbf{r}'|}, \quad (10.1)$$

$$M_{ij}^{II} = (\mathbf{i}_i \cdot \mathbf{i}_j) C_{ij}, \quad M_{ij}^{IS} = \bar{\sigma}_j (\mathbf{i}_i \cdot \nabla \phi_j^S) C_{ij}, \quad M_{ij}^{SS} = \bar{\sigma}_i \bar{\sigma}_j (\nabla \phi_i^S \cdot \nabla \phi_j^S) C_{ij} \quad (10.2)$$

(integration is performed over surfaces of two triangles) used for calculation of mutual inductance M_{ij}^{II} between the divergence-free currents (as in SHL and STARWALL). The additional mutual inductances M_{ij}^{IS} between eddy currents and source/sink currents, and M_{ij}^{SS} between source/sink currents use the same C_{ij} . This common feature provides the basis for interfacing upon necessity of the SSC and SHL codes with other similar codes, like STARWALL, or source/sink codes which are under development with an alternative approach.

The optimized formulation of the S/S-current problem for the typical tokamak situation of a localized wetting zone is presented. It is shown that the gradient representation can be used only in the wetting zone while the divergence-free stream function representation of the surface current can be used over the entire wall surface.

The numerical examples presented in the paper correspond to typical geometries of the wall and the wetting zone. In particular, the S/S and eddy currents generated by the Hiro current from the wall touching kink mode are modeled by both SSC and SHL codes.

Although the primary topic of the paper is the demonstration of capabilities of two numerical codes in modeling the currents in 3-dimensional walls the simulations of the WTKM give the strong support to the idea of explaining the negative voltage spike in tokamak disruptions by Hiro current excitation. This provides the additional motivation for further development of the presented model and the codes, which the authors consider

as an substantial but still incomplete step in simulations of electro-magnetic plasma-wall interactions.

In a next step, our approach of surface currents calculation can be included in the JOREK code (Huysmans *et al.* 2007; Hoelzl, *et al.* 2012; Hoelzl *et al.* 2014) for non-linear simulations of MHD instabilities in tokamaks.

Acknowledgement

This work is partially supported by US DoE contract No. DE-AC02-09-CH11466. C.V.A., K.L., M.H. and E.S. have carried this work out within the framework of the EUROfusion Consortium and has received funding from the European Union's Horizon 2020 research and innovation programme under grant agreement number 633053. The views and opinions expressed herein do not necessarily reflect those of the European Commission.

The stimulating discussions with David Coster are greatly appreciated.

REFERENCES

- LITUNOVSKI, R. 1995 The observation of phenomena during plasma disruption and the interpretation of the phenomena from the point of view of the toroidal asymmetry of forces., *JET Internal Report Contract No. JQ5/11961*.
- NOLL, P., ANDREW, P., BUZIO, M., LITUNOVSKI, R., RAIMONDI, T., RICCARDO, V. & VERRECCHIA, M. 1996 Present understanding of electromagnetic behaviour during disruptions at JET. In *Proc. 19th Symp. on Fusion Technology, Lisbon* (ed. C. Varandas & F. Serra), Amsterdam, **1**, 751. Elsevier.
- RICCARDO, V., NOLL, P. & WALKER, S. P. 2000 Forces between plasma, vessel and TF coils during AVDEs at JET. *Nucl. Fusion* **40**, 1805.
- RICCARDO, V. & WALKER, S. P. 2000 Parametric analysis of asymmetric vertical displacement events at JET. *Plasma Phys. Controlled Fusion* **42**, 29.
- RICCARDO, V. *et al.* 2009 Progress in understanding halo current at JET. *Nucl. Fusion* **49**, 055012.
- BACHMANN, C. *et al.* 2009 Specification of asymmetric VDE loads of the ITER tokamak. *Fusion Eng. and Des.* **86**, 1915.
- ZAKHAROV, L.E. 2008 The theory of the kink mode during the vertical plasma disruption events in tokamaks. *Phys. of Plasmas* **15**, 062507.
- ZAKHAROV, L.E., GALKIN, S. A., S. GERASIMOV, N., & JET-EFDA CONTRIBUTORS 2012 Understanding disruptions in tokamaks. *Phys. of Plasmas* **19**, 055703.
- GERASIMOV, S.N., HENDER, T.C., MORRIS, J., RICCARDO, V., ZAKHAROV, L.E. AND JET EFDA CONTRIBUTORS. (2014) Plasma current asymmetries during disruptions in JET. *Nucl. Fusion* **54** 073009
- XIONG, H., XU, G., WANG, H., ZAKHAROV, L.E. & LI, X. 2015 First measurements of Hiro currents in vertical displacement event in tokamaks. *Phys. Plasmas* **22**, 060702.
- GERASIMOV, S.N., ABREU, P., BARUZZO, M., DROZDOV, V., DVORNOVA, A., HAVLICEK, J., HENDER, T.C., HRONOVA, O., KRUEZI, U., LI, X., MARKOVIC, T., PNEK, R., RUBINACCI, G., TSALAS, M., VENTRE, S., VILLONE, F., ZAKHAROV, L.E. AND JET EFDA CONTRIBUTORS. (2015) JET and COMPASS asymmetrical disruptions. *Nucl. Fusion* **55** 113006
- ZAKHAROV, L.E. & LI, X. 2015 Tokamak magneto-hydrodynamics and reference magnetic coordinates for simulations of plasma disruptions. *Phys. of Plasmas* **22**, 062511.
- BERZAK HOPKINS, L., MENARD, J., MAJESKI, R., LUNDBERG, D.P., GRANSTEDT, E., JACOBSON, C., KAITA, R., KOZUB, T. & ZAKHAROV, L.E. 2012 Plasma equilibrium reconstructions in the lithium tokamak experiment. *Nucl. Fusion* **52**, 063025.
- MERKEL, P., NÜHRENBURG, C. & STRUMBERGER, E. 2004 Resistive Wall Modes of 3D Equilibria with Multiply-connected Walls. *31 st. EPS Conference on Plasma Physics. Europhys. Conf. Abstracts* **28G**, P1.208.

- MERKEL, P. & SEMPFF, M. 2006 Feedback Stabilization of Resistive Wall Modes in the Presence of Multiply connected Wall Structures. (*TH/P3-8*) *Procs. 21st IAEA Fusion Energy Conference, Chengdu, China, 2006*.
- STRUMBERGER, E., MERKEL, P., SEMPFF, M. & GÜNTER, S. 2008 On fully three-dimensional resistive wall mode and feedback stabilization computations. *Phys. Plasmas* **15**, 056110.
- TSEITLIN, L.A. 1970 Eddy Currents in Thin Plates and Shells. *Soviet Physics-Technical Physics* **10**, 1733.
- CHANCE, M.S. 1997 Vacuum calculations in azimuthally symmetric geometry. *Phys. Plasmas* **4**, 2161.
- CHANCE, M.S., CHU, M.S., OKABAYASHI, M. & TURNBULL, A.D. 2002 Theoretical modelling of the feedback stabilization of external MHD modes in toroidal geometry. *Nucl. Fusion* **42** 295.
- CHU, M.S., CHANCE, M.S., GLASSER, A.H. & OKABAYASHI, M. 2003 Normal mode approach to modelling of feedback stabilization of the resistive wall mode. *Nucl. Fusion* **43**, 441.
- IN, Y *et al.* 2009 Model-based dynamic resistive wall mode identification and feedback control in the DIII-D tokamak. *Phys. Plasmas* **13**, 062512.
- PUSTOVITOV, V.D. 2008 General formulation of the resistive wall mode coupling equations. *Phys. Plasmas* **15**, 072501.
- ATANASIU, C.V., MORARU, A. & ZAKHAROV, L.E. 2009 Influence of a Nonuniform Resistive Wall on the RWM Stability in a Tokamak., In *American Physical Society Plasma 51st Annual Meeting, Atlanta, USA, 2-6 November 2009*.
- ATANASIU, C.V. & ZAKHAROV, L.E. 2013 Response of a partial wall to an external perturbation of rotating plasma. *Phys. Plasmas* **20**, 092506.
- KUWAHARA, T. & TAKEDA, T. 1987 An effective analysis for three-dimensional boundary element method using analytically integrated higher order elements., *The Trans. of the Institute of Electrical Engineers of Japan* **107-A**, 275.
- G.T.A. HUYSMANS, G.T.A. & CZARNY, O. 2007 MHD stability in X-point geometry: simulation of ELMs, *Nucl. Fusion* **47** 659.
- MERKEL, P. & STRUMBERGER, E. 2015 Linear MHD stability studies with the STARWALL code. *arXiv:1508.04911*
- HOELZL, M., MERKEL, P., HUYSMANS, G.T.A., NARDON, E., MCADAMS, R. & CHAPMAN, I. 2012 Coupling the JOREK and STARWALL Codes for Non-linear Resistive-wall Simulations. *Journal of Physics: Conference Series*, **401**, 012010.
- HOELZL, M. *et al.* 2014, Non-Linear Simulations of MHD Instabilities in Tokamaks Including Eddy Current Effects and Perspectives for the Extension to Halo Currents. *Journal of Physics: Conference Series* **561**, 012011.